Journal of Russian Laser Research, Volume 33, Number 2, March, 2012

NONCOMMUTATIVE TOMOGRAPHY: A TOOL FOR DATA ANALYSIS AND SIGNAL PROCESSING

F. Briolle,[1] V. I. Man'ko,[2] B. Ricaud,[1] and R. Vilela Mendes[3,4*]

[1] *Centre de Physique Théorique*
CNRS Luminy, case 907, F-13288 Marseille Cedex 9, France
[2] *P. N. Lebedev Physical Institute, Russian Academy of Sciences*
Leninskii Prospect 53, Moscow 119991, Russia
[3] *CMAF, Instituto de Investigação Interdisciplinar, Universidade de Lisboa*
Av. Gama Pinto, 2 - P1649-003 Lisboa Codex, Portugal
[4] *IPFN, Instituto Superior Técnico*
Av. Rovisco Pais, Lisboa, Portugal

*Corresponding author e-mail: vilela@cii.fc.ul.pt
e-mails: Francoise.Briolle@univmed.fr; manko@sci.lebedev.ru; bricaud@cmi.univ-mrs.fr

Abstract

Tomograms, a generalization of the Radon transform to arbitrary pairs of noncommuting operators, are positive bilinear transforms with a rigorous probabilistic interpretation that provide a full characterization of the signal and are robust in the presence of noise. Tomograms, based on the time–frequency operator pair, were used in the past for a robust characterization of many different signals. Here we provide an explicit construction of tomogram transforms for many other pairs of noncommuting operators in one and two dimensions and describe how they are used for denoising, component separation, and filtering.

Keywords: bilinear transforms, tomograms, component separation, denoising.

1. Introduction

Integral transforms [1,2] are very useful for signal processing in communications, engineering, medicine, physics, etc. Linear and bilinear transforms have been used. Among the linear transforms, Fourier [3] and wavelets [4–6] are the most popular. Among the bilinear ones, the Wigner–Ville quasidistribution [7, 8] provides information in the joint time–frequency domain with good energy resolution. A joint time–frequency description of signals is important, because in many applications (biomedical, seismic, radar, etc.) the signals are of finite (sometimes very short) duration. However, the oscillating cross-terms in the Wigner–Ville quasidistribution make the interpretation of this transform a difficult matter. Even if the average of the cross-terms is small, their amplitude may be greater than the signal in time–frequency regions that carry no physical information. To profit from the time–frequency energy resolution of the bilinear transforms while controlling the cross-terms problem, modifications to the Wigner–Ville transform have been proposed. Transforms in the Cohen class [9, 10] make a two-dimensional filtering of the

Manuscript submitted by the authors in English on March 15, 2012.
1071-2836/12/3302-0103

Wigner–Ville quasidistribution, and the Gabor spectrogram [11] is a truncated version of this quasidistribution.

The difficulties with the physical interpretation of quasidistributions arise from the fact that time and frequency correspond to two noncommutative operators. Hence a joint probability density can never be defined. Even in the case of positive quasiprobabilities like the Husimi–Kano function [12, 13], an interpretation as a joint probability distribution is also not possible because the two arguments of the function are not simultaneously measurable random variables.

Recently, a new type of strictly positive bilinear transforms has been proposed [14, 15], called *tomograms*, which is a generalization of the Radon transform [16] to noncommutative pairs of operators. The Radon–Wigner transform [17, 18] is a particular case of such noncommutative tomography technique (see also some aspects of the technical applications in quantum mechanics [19]). The tomograms are strictly positive probability densities, provide a full characterization of the signal, and are robust in the presence of noise.

A unified framework to characterize linear transforms, quasidistributions, and tomograms was developed in [15]. This is briefly summarized in Sec. 2. Then Secs 3–7 contain an explicit construction of tomogram transforms for many pairs of noncommuting operators in one and two dimensions. Some of these transforms have been used in the past [20,21]; others are completely new. It is in the time–frequency plane that most signal-processing experts have developed their intuition, not in the eigenspaces associated to the new tomograms. Therefore, to provide a qualitative intuition on the way the tomograms explore the time–frequency plane, we have provided graphical spectrograms of the eigenstates on which the signal is projected by the tomograms. In Sec. 5, an interpretation of the tomograms is given as operator symbols of the set of projection operators in the space of signals. This provides a very general framework to deal with all kinds of custom-designed integral transforms both for deterministic and random signals. It also provides an alternative framework for an algebraic formulation of signal processing. Finally, we provide a detailed description of how tomograms may be used for denoising, component separation, and filtering of finite-time signals. The purpose of the present paper is to provide a unified mathematical construction of the tomogram transforms. For the specific applications of time–frequency tomograms, done in the past, we refer to [14, 20–23].

2. Linear Transforms, Quasidistributions, and Tomograms

Consider signals $f(t)$ as vectors $|f\rangle$ in a dense nuclear subspace $\mathcal{N}$ of a Hilbert space $\mathcal{H}$ with dual space $\mathcal{N}^*$ (with the canonical identification $\mathcal{N} \subset \mathcal{N}^*$) and a family of operators $\{U(\alpha) : \alpha \in I, I \subset \mathbb{R}^n\}$ defined on $\mathcal{N}^*$. In most cases of interest, $U(\alpha)$ generates a unitary group $U(\alpha) = e^{iB(\alpha)}$. Whenever a ket-bra notation is used, $|f\rangle \in \mathcal{N}$ and $\langle f| \in \mathcal{N}^*$. In this setting, three types of integral transforms are constructed.

Let $\langle h | \in \mathcal{N}^*$ be a reference vector and let U be such that the linear span of $\{\langle U(\alpha)h | \in \mathcal{N}^* : \alpha \in I\}$ is dense in $\mathcal{N}^*$. In $\{\langle U(\alpha)h |\}$, a complete set of vectors can be chosen to serve as basis.

1 - Linear Transforms

$$W_f^{(h)}(\alpha) = \langle U(\alpha)\, h \mid f\rangle. \tag{1}$$

2 - Quasidistributions

$$Q_f(\alpha) = \langle U(\alpha)\, f \mid f\rangle. \tag{2}$$

3 - Tomograms

If $U(\alpha)$ is a unitary operator, there is a self-adjoint operator $B(\alpha)$ such that $U(\alpha) = e^{iB(\alpha)}$, with $B(\alpha)$ having a spectral projection $B(\alpha) = \int XP(X)\,dX$. Let $P(X) \doteq |X\rangle\langle X|$ be the projector* on the (generalized) eigenvector $\langle X| \in \mathcal{N}^*$ of $B(\alpha)$. Then the tomogram is

$$M_f^{(B)}(X) = \langle f|\,P(X)\,|f\rangle = \langle f|\,X\rangle\langle X\,|f\rangle = |\langle X\,|f\rangle|^2 . \tag{3}$$

Therefore, the tomogram $M_f^{(B)}(X)$ is the squared amplitude of the projection of the signal $|f\rangle \in \mathcal{N}$ on the eigenvector $\langle X| \in \mathcal{N}^*$ of the operator $B(\alpha)$, putting in evidence the positivity of the tomogram. Furthermore, for normalized $\mid f\rangle$, $\langle f \mid f\rangle = 1$, the tomogram is normalized $\int M_f^{(B)}(X)\,dX = 1$, and is interpreted as a probability distribution on the set of generalized eigenvalues of $B(\alpha)$, that is, a probability distribution for the random variable X corresponding to the observable defined by the operator $B(\alpha)$.

If, by a unitary transform S, $B(\alpha)$ is transformed to $SB(\alpha)S^\dagger = B'(\alpha)$, and $\{\mid Z\rangle\}$ is the set of (generalized) eigenvectors of $B'(\alpha)$, $\left\{S^\dagger \mid Z\rangle\right\}$ is the set of eigenvectors for B. Therefore,

$$M_f^{(B)}(Z) = \langle f \mid S^\dagger \mid Z\rangle\langle Z \mid S \mid f\rangle = |\langle Z \mid S \mid f\rangle|^2.$$

The tomogram is a homogeneous function $M_f^{(B/p)}(X) = |p| M_f^{(B)}(pX)$.

Examples:

If $U(\alpha)$ is unitary generated by $B_F(\overrightarrow{\alpha}) = \alpha_1 t + i\alpha_2 \dfrac{d}{dt}$ and h is a (generalized) eigenvector of the time-translation operator, the linear transform $W_f^{(h)}(\alpha)$ is the Fourier transform. For the same $B_F(\overrightarrow{\alpha})$, the quasidistribution $Q_f(\alpha)$ is the ambiguity function.

The Wigner–Ville transform [7,8] is the quasidistribution $Q_f(\alpha)$ for the following B-operator:

$$B^{(\mathrm{WV})}(\alpha_1, \alpha_2) = -i2\alpha_1 \frac{d}{dt} - 2\alpha_2 t + \frac{\pi\left(t^2 - \dfrac{d^2}{dt^2} - 1\right)}{2} . \tag{4}$$

The wavelet transform is $W_f^{(h)}(\alpha)$ for $B_W(\overrightarrow{\alpha}) = \alpha_1 D + i\alpha_2 \dfrac{d}{dt}$, with D being the dilation operator $D = -\dfrac{1}{2}\left(it\dfrac{d}{dt} + i\dfrac{d}{dt}t\right)$. The wavelets $h_{s,\tau}(t)$ are kernel functions generated from a basic wavelet $h(\tau)$ by means of a translation and a rescaling ($-\infty < \tau < \infty$, $s > 0$),

$$h_{s,\tau}(t) = \frac{1}{\sqrt{s}}\, h\left(\frac{t-\tau}{s}\right). \tag{5}$$

Using the operator

$$U^{(A)}(\tau, s) = \exp(i\tau\hat{\omega})\exp(i\log sD), \tag{6}$$

we have

$$h_{s,\tau}(t) = U^{(A)\dagger}(\tau, s)h(t). \tag{7}$$

*Another convenient notation for the projector on a generalized eigenvector of $B(\alpha)$ with eigenvalue X is $\delta(B(\alpha) - X) \doteq P(X)$.

For normalized $h(t)$, the wavelets $h_{s,\tau}(t)$ satisfy the normalization condition $\int |h_{s,\tau}(t)|^2\,dt = 1$. The basic wavelet (reference vector) may have different forms, for example,

$$h(t) = \frac{1}{\sqrt{\pi}}\,e^{i\omega_0 t}\,e^{-t^2/2}, \tag{8}$$

or

$$h(t) = (1-t^2)\,e^{-t^2/2} \tag{9}$$

called the Mexican hat wavelet.

The Bertrand transform [24,25] is $Q_f(\alpha)$ for B_W.

Linear, bilinear, and tomogram transforms are related to one another as follows:

$$M_f^{(B)}(X) = \frac{1}{2\pi}\int Q_f^{(kB)}(\alpha)\,e^{-ikX}\,dk, \qquad Q_f^{(B)}(\alpha) = \int M_f^{(B/p)}(X)\,e^{ipX}\,dX,$$
$$Q_f^{(B)}(\alpha) = W_f^{(f)}(\alpha), \qquad W_f^{(h)}(\alpha) = \frac{1}{4}\int e^{iX}\left[\begin{array}{c} M_{f_1}^{(B)}(X) - iM_{f_2}^{(B)}(X) \\ -M_{f_3}^{(B)}(X) + iM_{f_4}^{(B)}(X) \end{array}\right] dX,$$

with $\mid f_1\rangle = \mid h\rangle + \mid f\rangle$, $\mid f_3\rangle = \mid h\rangle - \mid f\rangle$, $\mid f_2\rangle = \mid h\rangle + i\mid f\rangle$, and $\mid f_4\rangle = \mid h\rangle - i\mid f\rangle$.

3. One-Dimensional Tomograms

As shown in (3), a tomogram corresponds to projections on the eigenstates of the B operators. These operators are linear combinations of different (commuting or noncommuting) operators, $B = \mu O_1 + \nu O_2$. Therefore, the tomogram explores the signal along lines in the plane (O_1, O_2). For example, for

$$B\,(\mu,\nu) = \mu t + \nu\omega = \mu t + i\nu\frac{d}{dt}\,,$$

the tomogram is the expectation value of a projection operator with support on a line in the time–frequency plane $X = \mu t + \nu\omega$. Therefore, $M_f^{(S)}(X,\mu,\nu)$ is the marginal distribution of the variable X along this line in the time–frequency plane. The line is rotated and rescaled when one changes the parameters μ and ν. In this way, the whole time–frequency plane is sampled, and the tomographic transform contains all information on the signal.

It is clear that, instead of marginals collected along straight lines on the time–frequency plane, one may use other curves to sample this space. It has been shown in [15] that the tomograms associated to the affine group, when

$$B\,(\mu,\nu) = \mu t + \nu\frac{t\omega + \omega t}{2}\,, \tag{10}$$

correspond to hyperbolas in the time–frequency plane. This point of view has been further explored in [26] defining tomograms in terms of marginals over surfaces generated by deformations of families of hyperplanes or quadrics. However, not all tomograms may be defined as marginals on lines in the time–frequency plane.

Here we construct the tomograms corresponding to a large set of operators. Of particular interest are the tomograms associated to finite-dimensional Lie algebras.

3.1. 1D Conformal Group Tomograms

The generators of the one-dimensional conformal group are

$$\omega = i\frac{d}{dt}, \qquad D = i\left(t\frac{d}{dt} + \frac{1}{2}\right), \qquad K = i\left(t^2\frac{d}{dt} + t\right). \tag{11}$$

One may construct tomograms using the following operators:

Time–frequency

$$B_1 = \mu t + i\nu\frac{d}{dt}; \tag{12}$$

Time–scale

$$B_2 = \mu t + i\nu\left(t\frac{d}{dt} + \frac{1}{2}\right); \tag{13}$$

Frequency–scale

$$B_3 = i\mu\frac{d}{dt} + i\nu\left(t\frac{d}{dt} + \frac{1}{2}\right); \tag{14}$$

Time–conformal

$$B_4 = \mu t + i\nu\left(t^2\frac{d}{dt} + t\right). \tag{15}$$

The construction of the tomograms reduces to calculating the generalized eigenvectors of each one of the B_i operators:

$B_1\psi_1(\mu,\nu,t,X) = X\psi_1(\mu,\nu,t,X)$,

$$\psi_1(\mu,\nu,t,X) = \exp i\left(\frac{\mu t^2}{2\nu} - \frac{tX}{\nu}\right), \tag{16}$$

with normalization

$$\int dt\, \psi_1^*(\mu,\nu,t,X)\,\psi_1(\mu,\nu,t,X') = 2\pi\nu\delta(X - X'); \tag{17}$$

$B_2\psi_2(\mu,\nu,t,X) = X\psi_2(\mu,\nu,t,X)$,

$$\psi_2(\mu,\nu,t,X) = \frac{1}{\sqrt{|t|}}\exp i\left(\frac{\mu t}{\nu} - \frac{X}{\nu}\log|t|\right), \tag{18}$$

with normalization

$$\int dt\, \psi_2^*(\mu,\nu,t,X)\,\psi_2(\mu,\nu,t,X') = 4\pi\nu\delta(X - X'); \tag{19}$$

$B_3\psi_3(\mu,\nu,\omega,X) = X\psi_3(\mu,\nu,\omega,X)$,

$$\psi_3(\mu,\nu,t,X) = \exp(-i)\left(\frac{\mu}{\nu}\omega - \frac{X}{\nu}\log|\omega|\right), \tag{20}$$

with normalization

$$\int d\omega\, \psi_1^*(\mu,\nu,\omega,X)\,\psi_1(\mu,\nu,\omega,X') = 2\pi\nu\delta(X - X'); \tag{21}$$

$$B_4\psi_4\left(\mu,\nu,t,X\right)=X\psi_4\left(\mu,\nu,t,X\right),$$

$$\psi_4\left(\mu,\nu,t,X\right)=\frac{1}{|t|}\exp i\left(\frac{X}{\nu t}+\frac{\mu}{\nu}\log|t|\right), \tag{22}$$

with normalization

$$\int dt\,\psi_4^*\left(\mu,\nu,t,s\right)\psi_4\left(\mu,\nu,t,s'\right)=2\pi\nu\delta\left(s-s'\right). \tag{23}$$

Then the tomograms are

Time–frequency tomogram

$$M_1\left(\mu,\nu,X\right)=\frac{1}{2\,\pi|\nu|}\left|\int\exp\left[\frac{i\mu t^2}{2\,\nu}-\frac{itX}{\nu}\right]f(t)\,dt\right|^2; \tag{24}$$

Time–scale tomogram

$$M_2(\mu,\nu,X)=\frac{1}{2\pi|\nu|}\left|\int dt\,\frac{f(t)}{\sqrt{|t|}}\exp\left\{\left[i\left(\frac{\mu}{\nu}t-\frac{X}{\nu}\log|t|\right)\right]\right\}\right|^2; \tag{25}$$

Frequency–scale tomogram

$$M_3(\mu,\nu,X)=\frac{1}{2\pi|\nu|}\left|\int d\omega\,\frac{f(\omega)}{\sqrt{|\omega|}}\exp\left\{\left[-i\left(\frac{\mu}{\nu}\omega-\frac{X}{\nu}\log|\omega|\right)\right]\right\}\right|^2, \tag{26}$$

with $f(\omega)$ being the Fourier transform of $f(t)$;

Time–conformal tomogram

$$M_4(\mu,\nu,X)=\frac{1}{2\pi|\nu|}\left|\int dt\,\frac{f(t)}{|t|}\exp\left\{\left[i\left(\frac{X}{\nu t}+\frac{\mu}{\nu}\log|t|\right)\right]\right\}\right|^2. \tag{27}$$

The tomograms M_1, M_2, and M_4 interpolate between the (squared) time signal and its projection on the $\psi_i\left(\mu,\nu,t,X\right)$ functions for $\mu=0$. Figure 1 shows the typical behavior of the real part of these functions.

Figures 2–4 illustrate how the tomograms M_1, M_2, and M_4 explore the time–frequency space by plotting the spectrograms of typical vectors ψ_1, ψ_2, and ψ_4.

In a similar way, tomograms may be constructed for any operator of the general type

$$B_4=\mu t+i\nu\left(g\left(t\right)\frac{d}{dt}+\frac{1}{2}\frac{dg\left(t\right)}{dt}\right),$$

the generalized eigenvectors being

$$\psi_g\left(\mu,\nu,t,X\right)=\left|g\left(t\right)\right|^{-1/2}\exp i\left(-\frac{X}{\nu}\int^t\frac{ds}{g\left(s\right)}+\frac{\mu}{\nu}\int^t\frac{s\,ds}{g\left(s\right)}\right).$$

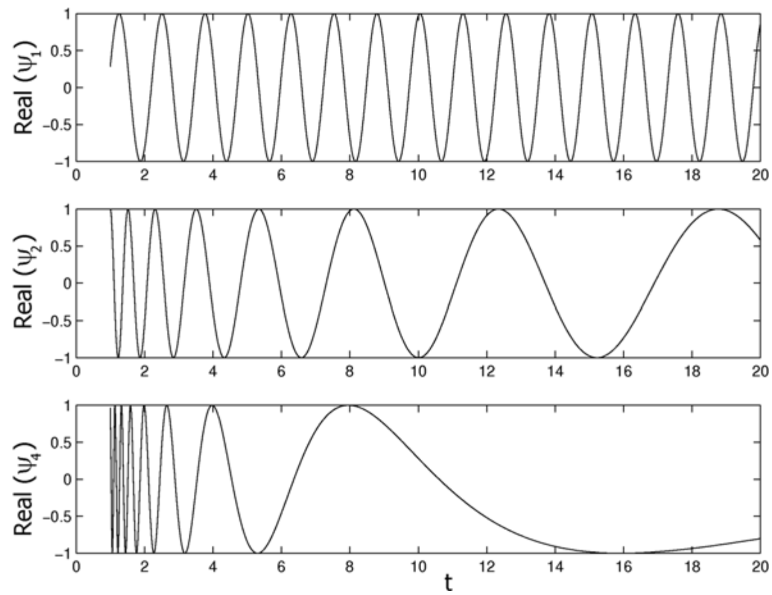

Fig. 1. Typical behavior of the real part of the functions ψ_1, ψ_2, and ψ_4 at $\mu = 0$.

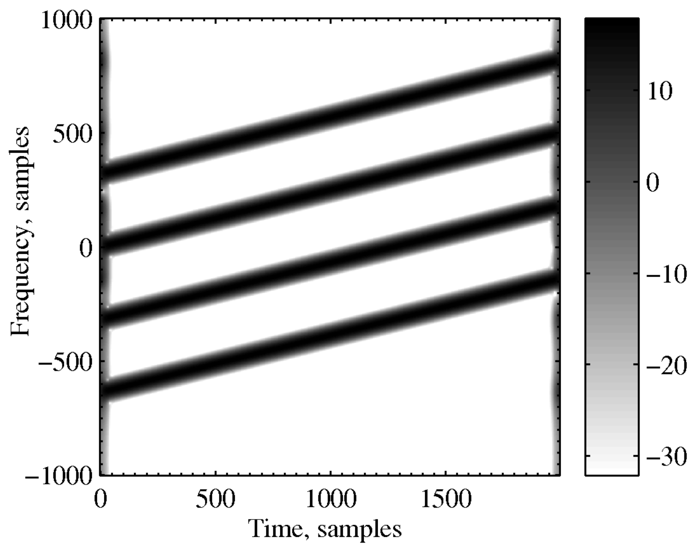

Fig. 2. Modulus of the short-time Fourier transform of four vectors of the time–frequency tomogram for some fixed θ, $\mu = \cos\theta$, and $\nu = \sin\theta$. A vector is a linear chirp, hence a line in the time–frequency plane. Moreover, each vector is a frequency-translated version of the one which starts at the origin. Since it forms an orthogonal basis, the sum of all the vectors covers the entire time–frequency plane. The parameter θ allows one to change the slope of the line in the time–frequency plane.

3.2. Another Finite-Dimensional Algebra

Another finite-dimensional Lie algebra that may be used to construct tomograms, exploring other features of the signals, is generated by $\mathbf{1}$, t, and

$$\omega = i\frac{d}{dt}, \qquad D = i\left(t\frac{d}{dt} + \frac{1}{2}\right), \qquad F = -\frac{1}{2}\left(\frac{d^2}{dt^2} - t^2 + 1\right), \qquad \sigma = \frac{1}{2}\left(\frac{d^2}{dt^2} + t^2 + 1\right).$$

Of special interest are the tomograms related to the operators $B_F = \mu t + \nu F$ and $B_\sigma = \mu t + \nu\sigma$.

As before, the construction of the tomograms relies on finding a complete set of generalized eigenvectors for the operators B_F and B_σ. With $y = t + \mu/\nu$, one defines the creation and annihilation operators

$$a = \frac{1}{\sqrt{2}}\left(y + \frac{d}{dy}\right), \qquad a^\dagger = \frac{1}{\sqrt{2}}\left(y - \frac{d}{dy}\right),$$

obtaining

$$B_F = \nu\left(a^\dagger a - \mu^2/2\nu^2\right), \qquad B_\sigma = \nu\left(aa - \mu^2/2\nu^2\right).$$

Therefore, for B_F one has an orthonormalized complete set of eigenvectors $\psi_n^{(F)}(t) = u_n(t + \mu/\nu)$, with

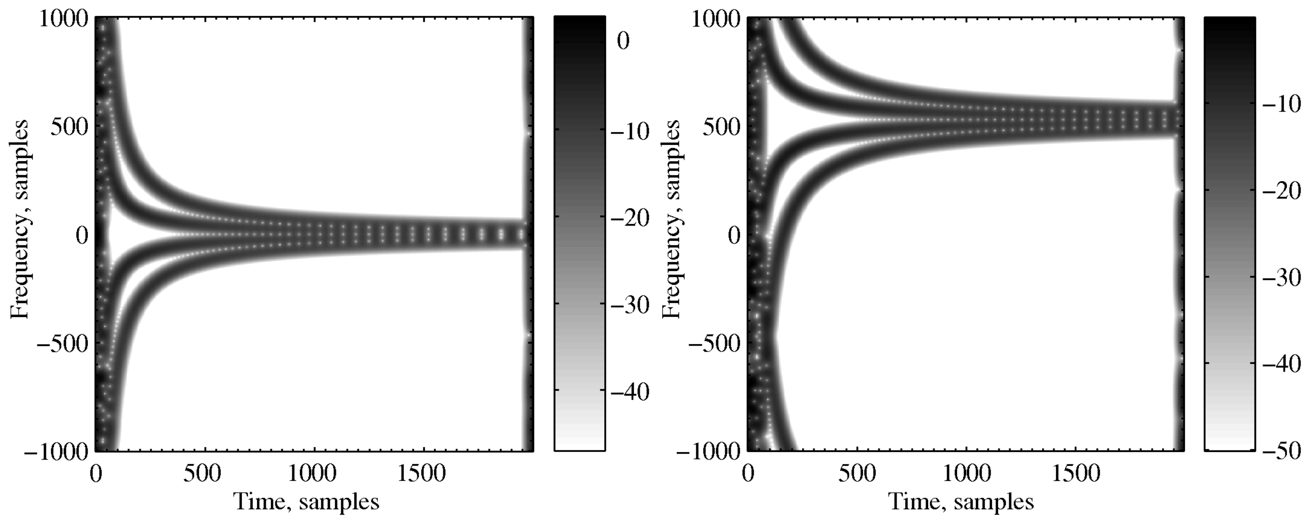

Fig. 3. Modulus of the short-time Fourier transform of four vectors of the time–scale tomogram for $\mu = 0$, $\nu = 1$ (left) and $\mu = \sqrt(2)/2$, $\nu = \sqrt(2)/2$ (right). Each vector is an hyperbolic chirp. Two of them correspond to positive X and two of them to negative X. Due to the sampling used in the numerical computation, some aliasing phenomenon occurs at times close to zero. There is an axis of symmetry – the line of zero frequency on the left graph. This axis is shifted in frequency when μ and ν are changed.

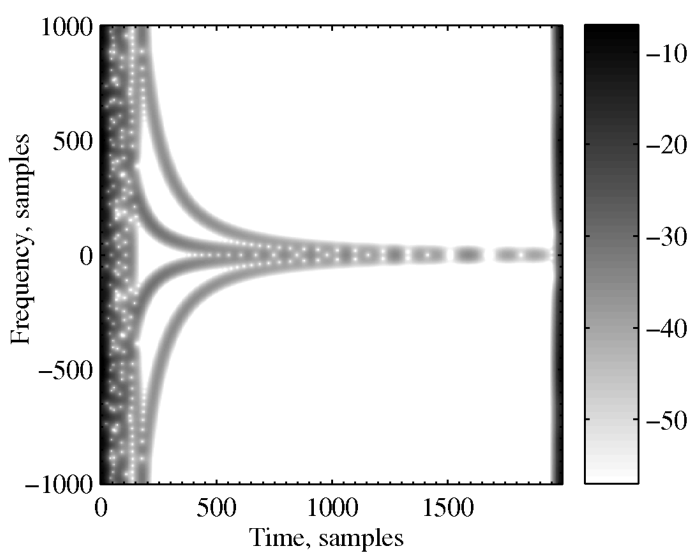

Fig. 4. Modulus of the short-time Fourier transform of four vectors of the time–conformal tomogram for $\mu = 0$ and $\nu = 1$. Due to the sampling used in the numerical computation, some aliasing phenomenon occurs at times close to zero. Some interferences between the vectors occur for large time. Two vectors correspond to positive X and two to negative X.

a discrete set of eigenvalues $B_F\psi_n^{(F)}(t) = X_n\psi_n^{(F)}(t)$, $X_n = \nu(n+1/2) - \mu^2/2\nu$, the function u_n being $u_n(y) = \left(\pi^{1/2}2^n n!\right)^{-1/2}\left(y - \frac{d}{dy}\right)^n e^{-y^2/2}$. The tomogram $M_f^{(F)}(\mu,\nu,X_n)$ is

$$M_f^{(F)}(\mu,\nu,X_n) = \left|\int \psi_n^{(F)*}(t)\, f(t)\, dt\right|^2.$$

For B_σ, one uses a basis of coherent states

$$\phi_\lambda(y) = e^{\lambda a^\dagger - \lambda^* a}u_0(y) = e^{|\lambda|^2/2}\sum_{n=0}\frac{\lambda^n}{\sqrt{n!}}u_n(y),$$

with decomposition of identity $\frac{1}{\pi}\int \phi_\lambda(y)\,\phi_\lambda^*(y)\,d^2\lambda = 1$. Then, a set of generalized eigenstates of B_σ is $\psi_\lambda^{(\sigma)}(\mu,\nu,t) = \phi_\lambda(t+\mu/\nu)$. With eigenvalues $B_\sigma\psi_\lambda^{(\sigma)}(\mu,\nu,t) = X_\lambda\psi_\lambda^{(\sigma)}(\mu,\nu,t)$, $X_\lambda = \nu\left(\lambda^2 - \mu^2/2\nu^2\right)$, the tomogram reads

$$M_f^{(\sigma)}(\mu,\nu,X_\lambda) = \left|\int \psi_\lambda^{(\sigma)*}(\mu,\nu,t)\, f(t)\, dt\right|^2.$$

This tomogram is closely related to the Sudarshan–Glauber P-representation [27–29].

4. Multidimensional Tomograms

Several types of multidimensional tomograms may be obtained from generalizations of the one-dimensional ones. Consider a signal $f(t_1,t_2)$. The tomogram depends on a vector variable $\vec{X} = (X_1, X_2)$ and four real parameters μ_1, μ_2, ν_1, and ν_2. For example, the two-dimensional time–frequency tomogram reads

$$M(\vec{X},\vec{\mu},\vec{\nu}) = \frac{1}{2\pi|\nu_1|}\,\frac{1}{2\pi|\nu_2|}\left|\iint f(t_1,t_2)\exp\left(\frac{i\mu_1}{2\nu_1}\,t_1^2 - \frac{iX_1}{\nu_1}\,t_1 + \frac{i\mu_2}{2\nu_2}\,t_2^2 - \frac{iX_2}{\nu_2}\,t_2\right)dt_1\,dt_2\right|^2. \tag{28}$$

From this, one may also construct a *center-of-mass tomogram*

$$M_{\rm cm}(Y,\vec{\mu},\vec{\nu}) = \int M(\vec{X},\vec{\mu},\vec{\nu})\,\delta(Y - X_1 - X_2)\,dX_1\,dX_2 = \int \delta(Y - X_1 - X_2)\,\frac{1}{2\pi|\nu_1|}\,\frac{1}{2\pi|\nu_2|}$$
$$\times\left|\iint f(t_1,t_2)dt_1\,dt_2\,\exp\left(\frac{i\mu_1}{2\nu_1}\,t_1^2 - \frac{it_1X_1}{\nu_1} + \frac{i\mu_2}{2\nu_2}\,t_2^2 - \frac{it_2X_2}{\nu_2}\right)\right|^2 dX_1\,dX_2.$$

The center-of-mass tomogram is normalized $\int M_{\rm cm}(X,\vec{\mu},\vec{\nu})\,dX = 1$ and a homogeneous function $M_{\rm cm}(\lambda X,\lambda\vec{\mu},\lambda\vec{\nu}) = \frac{1}{|\lambda|}\,M_{\rm cm}(X,\vec{\mu},\vec{\nu})$. The generalization to N channels is straightforward.

As in the one-dimensional case, useful tomograms may be constructed from the operators of Lie algebras. For example, from the generators of the conformal algebra in $\mathbb{R}^d$, $d \geq 2$,

$$\omega_k = i\frac{\partial}{\partial t_k}, \qquad D = i\left(t\bullet\nabla + \frac{d}{2}\right), \qquad R_{j,k} = i\left(t_j\frac{\partial}{\partial t_k} - t_k\frac{\partial}{\partial t_j}\right), \qquad K_j = i\left(t_j^2\frac{\partial}{\partial t_j} + t_j\right).$$

Let, in two dimensions, $t_1 = t$ and $t_2 = x$. The tomograms, corresponding to the operators

$$B_\omega = \mu_1 t + \mu_2 x + \nu_1\omega_1 + \nu_2\omega_2, \qquad B_D = \mu_1 t + \mu_2 x + \nu D, \qquad B_\omega = \mu_1 t + \mu_2 x + \nu_1 K_1 + \nu_2 K_2,$$

are, as in (28), straightforward generalizations of the corresponding one-dimensional ones.

For the operator $B_R = \mu_1 t + \mu_2 x + \nu R_{1,2}$, the eigenstates are

$$\psi^{(R)}\left(\vec{\mu}, \nu, x, t, X\right) = \exp\frac{i}{\nu}\left(\mu_1 x - \mu_2 t + X\tan^{-1}\frac{t}{x}\right),$$

and the tomogram reads

$$M_f\left(\vec{\mu}, \nu, X\right) = \left|\int \psi^{(R)*}\left(\vec{\mu}, \nu, x, t, X\right) f\left(x, t\right) dx\, dt\right|^2.$$

5. The Tomograms as Operator Symbols

Tomograms may be described not only as amplitudes of projections on a complete basis of eigenvectors of a family of operators, but also as operator symbols. That is, as a map of operators to a space of functions where the operators noncommutativity is replaced by a modification of the usual product to a star-product.

Let $\hat{A}$ be an operator in the Hilbert space $\mathcal{H}$, and $\hat{U}(\vec{x})$ and $\hat{D}(\vec{x})$ two families of operators called *dequantizers* and *quantizers*, respectively, such that (see, e.g., [30])

$$\mathrm{Tr}\left\{\hat{U}(\vec{x})\hat{D}(\vec{x}\,')\right\} = \delta(\vec{x} - \vec{x}\,'). \tag{29}$$

The labels $\vec{x}$ (with components $x_1, x_2, \ldots, x_n$) are coordinates in a linear space V where the functions (operator symbols) are defined. Some of the coordinates may take discrete values, then the delta-function in (29) should be understood as a Kronecker delta. Provided the property (29) is satisfied, one defines the *symbol of the operator* $\hat{A}$ by the formula

$$f_A(\vec{x}) = \mathrm{Tr}\left\{\hat{U}(\vec{x})\hat{A}\right\}, \tag{30}$$

assuming the trace to exist. In view of (29), one has the reconstruction formula $\hat{A} = \int f_A(x)\hat{D}(\vec{x})\, d\vec{x}$. The role of quantizers and dequantizers may be exchanged. Then $f_A^d(\vec{x}) = \mathrm{Tr}\left\{\hat{D}(\vec{x})\,\hat{A}\right\}$ is called the dual symbol of $f_A(\vec{x})$, and the reconstruction formula is $\hat{A} = \int f_A^d(x)\hat{U}(\vec{x})\, d\vec{x}$. Symbols of operators can be multiplied using the star-product kernel as follows:

$$f_A(\vec{x}) \star f_B(\vec{x}) = \int f_A(\vec{y}) f_B(\vec{z}) K(\vec{y}, \vec{z}, \vec{x})\, d\vec{y}\, d\vec{z}, \tag{31}$$

the kernel being $K(\vec{y}, \vec{z}, \vec{x}) = \mathrm{Tr}\left\{\hat{D}(\vec{y})\hat{D}(\vec{z})\hat{U}(\vec{x})\right\}$. The star-product is associative,

$$\left(f_A(\vec{x}) \star f_B(\vec{x})\right) \star f_C(\vec{x}) = f_A(\vec{x}) \star \left(f_B(\vec{x}) \star f_C(\vec{x})\right), \tag{32}$$

and this property corresponds to the associativity of the product of operators in the Hilbert space.

With the dual symbols, the trace of an operator may be written in integral form

$$\mathrm{Tr}\left\{\hat{A}\hat{B}\right\} = \int f_A^d(\vec{x}) f_B(\vec{x})\, d\vec{x} = \int f_B^d(\vec{x}) f_A(\vec{x})\, d\vec{x}. \tag{33}$$

For two different symbols $f_A(\vec{x})$ and $f_A(\vec{y})$ corresponding, respectively, to the pairs $\left(\hat{U}(\vec{x}), \hat{D}(\vec{x})\right)$ and $\left(\hat{U}_1(\vec{y}), \hat{D}_1(\vec{y})\right)$, one has the relation $f_A(\vec{x}) = \int f_A(\vec{y}) K(\vec{x},\vec{y})\, d\vec{y}$, with intertwining kernel $K(\vec{x},\vec{y}) = \mathrm{Tr}\left\{\hat{D}_1(\vec{y})\hat{U}(\vec{x})\right\}$.

Let now each signal $f(t)$ be identified with the projection operator Π_f on the function $f(t)$, denoted by

$$\Pi_f = |f\rangle\langle f|\,. \tag{34}$$

Then the tomograms, and also other transforms, are symbols of the projection operators for several choices of quantizers and dequantizers.

Some Examples:

The *Wigner–Ville function* is the symbol of $| f\rangle\langle f |$ corresponding to the dequantizer

$$\hat{U}(\vec{x}) = 2\hat{\mathcal{D}}(2\alpha)\hat{P}, \qquad \alpha = \frac{t+i\omega}{\sqrt{2}}\,, \tag{35}$$

where $\hat{P}$ is the inversion operator $\hat{P}f(t) = f(-t)$, and $\hat{\mathcal{D}}(\gamma)$ is a displacement operator,

$$\hat{\mathcal{D}}(\gamma) = \exp\left[\frac{1}{\sqrt{2}}\gamma\left(t - \frac{\partial}{\partial t}\right) - \frac{1}{\sqrt{2}}\gamma^*\left(t + \frac{\partial}{\partial t}\right)\right]. \tag{36}$$

The quantizer operator reads

$$\hat{D}(\vec{x}) := \hat{D}(t,\omega) = \frac{1}{2\pi}\hat{U}(t,\omega), \tag{37}$$

with t and ω being time and frequency.

The Wigner–Ville function is

$$W(t,\omega) = 2\mathrm{Tr}\left\{| f\rangle\langle f |\, \hat{D}(2\alpha)\hat{P}\right\} \tag{38}$$

or, in integral form

$$W(t,\omega) = 2\int f^*(t)\hat{\mathcal{D}}(2\alpha) f(-t)\, dt. \tag{39}$$

The *symplectic tomogram* or time–frequency tomogram of $| f\rangle\langle f |$ corresponds to the dequantizer

$$\hat{U}(\vec{x}) := \hat{U}(X,\mu,\nu) = \delta\left(X\hat{1} - \mu\hat{t} - \nu\hat{\omega}\right), \tag{40}$$

where the notation $\delta\left(X\hat{1} - \mu\hat{t} - \nu\hat{\omega}\right)$ stands for the projector on the eigenvector of $\mu\hat{t}+\nu\hat{\omega}$ corresponding to the eigenvalue X,

$$\hat{t}f(t) = tf(t), \qquad \hat{\omega}f(t) = -i\frac{\partial}{\partial t}\, f(t), \tag{41}$$

and $X, \mu, \nu \in R$. The quantizer of the symplectic tomogram is

$$\hat{D}(\vec{x}) := \hat{D}(X, \mu, \nu) = \frac{1}{2\pi} \exp\left[i\left(X\hat{1} - \mu\hat{t} - \nu\hat{\omega}\right)\right]. \tag{42}$$

The *optical tomogram* is the same as above for the case $\mu = \cos\theta$ and $\nu = \sin\theta$.
Thus the optical tomogram reads

$$\begin{aligned} M(X,\theta) &= \mathrm{Tr}\left\{\mid f\rangle\langle f \mid \delta\left(X\hat{1} - \mu\hat{t} - \nu\hat{\omega}\right)\right\} \\ &= \frac{1}{2\pi}\int f^*(t)e^{ikX} \exp\left[ik\left(X - t\cos\theta + i\frac{\partial}{\partial t}\sin\theta\right)\right] f(t)\,dt\,dk \\ &= \frac{1}{2\pi|\sin\theta|}\left|\int f(t)\exp\left[i\left(\frac{\cot\theta}{2}t^2 - \frac{Xt}{\sin\theta}\right)\right]dt\right|^2. \end{aligned} \tag{43}$$

One important feature of the formulation of tomograms as operator symbols is that one may work with deterministic signals $f(t)$ as easily as with probabilistic ones. In this latter case, the projector in (34) would be replaced by

$$\Pi_p = \int p_\mu \left|f_\mu\right\rangle \left\langle f_\mu\right| \, d\mu, \tag{44}$$

with $\int p_\mu d\mu = 1$, the tomogram being the symbol of this new operator.

This also provides a framework for an algebraic formulation of signal processing, perhaps more general than the one described in [31, 32]. There, a signal model is a triple $(\mathcal{A}, \mathcal{M}, \Phi)$, with $\mathcal{A}$ being an algebra of linear filters, $\mathcal{M}$ a $\mathcal{A}$-module, and Φ a map from the vector space of signals to the module. With the operator symbol interpretation, both (deterministic or random) signals and (linear or nonlinear), transforms on signals are operators. By the application of the dequantizer [Eq. (30)], they are mapped onto functions, the filter operations becoming star-products.

6. Rotated-Time Tomography

Now we consider a version of tomography where a discrete random variable is used as an argument of the probability-distribution function. We call this tomography *rotated-time tomography.* It is a variant of the spin-tomographic approach for the description of discrete spin states in quantum mechanics. For a finite-duration signal $f(t)$, with $0 \leq t \leq T$, we consider discrete values of time $f(t_m) \equiv f_m$ where, with the labeling $m = -j, -j+1, -j+2, \ldots, 0, 1, \ldots, j-1, j$, they are like the components of a spinor $\mid f\rangle$. This means that we split the interval $[0, T]$ onto N parts at time values $t_{-j}, t_{-j+1}, \ldots, t_j$ and replace the signal $f(t)$, a function of continuous time, by a discrete set of values organized as a spinor. By dividing by a factor, we normalize the spinor, i.e., $\langle f \mid f\rangle = \sum_{m=-j}^{j} |f_m|^2 = 1$. Without loss of generality, we consider the "spin" values to be integers, i.e., $j = 0, 1, 2, \ldots$, and use an odd number $N = 2j+1$ of values.

In this setting, $\mid f\rangle$ being a column vector, we construct the $N\times N$ matrix $\rho = \mid f\rangle\langle f\mid$, with matrix elements $\rho_{mm'} = f_m f_{m'}^*$. The tomogram is defined as the probability-distribution function

$$\mathcal{M}(m, u) = |\langle m \mid u \mid f\rangle|^2, \qquad m = -j, \ldots, j-1, j, \tag{45}$$

where u is an unitary $N\times N$ matrix $uu^\dagger = 1_N$. For this matrix, we use an unitary irreducible representation of the rotation group [or $SU(2)$] with matrix elements

$$\begin{aligned} u_{mm'}(\theta) &= \frac{(-1)^{j-m'}}{(m+m')!}\left[\frac{(j+m)!(j+m')!}{(j-m)!(j-m')!}\right]^{1/2}\left(\sin\frac{\theta}{2}\right)^{m-m'}\left(\cos\frac{\theta}{2}\right)^{m+m'} \\ &\times\mathcal{F}_{j-m}\left(2m+1, m+m'^2\frac{\theta}{2}\right), \end{aligned} \tag{46}$$

with $\mathcal{F}_{j-m}$ being a function with the Jacobi-polynomial structure expressed in terms of hypergeometric functions as

$$\mathcal{F}_n(a,b,t) = F(-n,a+n,b;t) = \frac{(b-1)!}{(b+n-1)!}\,t^{1-b}(1-t)^{b-a}\left(\frac{d}{dt}\right)^n\left[t^{b+n-1}(1-t)^{a-b+1}\right]. \tag{47}$$

The dequantizer in the rotated-time tomography is

$$\hat{U}(\vec{x}) \equiv U(m,\vec{n}) = \delta(m1 - u^\dagger J_z u) = \delta\left(m1 - \vec{n}\vec{J}\right), \tag{48}$$

where J_z is the matrix with diagonal matrix elements $(J_z)_{mm'} = m\delta_{mm'}$.

The vector $\vec{n} = (\sin\theta\cos\varphi, \sin\theta\sin\varphi, \cos\theta)$ determines a direction in 3D space. The matrix (46) was written for $\varphi = 0$ but, if this angle is nonzero, the matrix element has to be multiplied by the phase factor $e^{im\varphi}$.

The quantizer can take several forms:

In integral form, it reads

$$\hat{D}(m,\vec{n}) = \frac{2j+1}{\pi}\int_0^{2\pi}\sin^2\frac{\gamma}{2}\exp(-i\vec{J}\vec{n})\gamma\,d\gamma(\cdots). \tag{49}$$

The tomogram $\mathcal{M}(m,u)$ is a nonnegative normalized probability distribution depending on the direction $\vec{n}$, i.e., $\mathcal{M}(m,u) \geq 0$ and $\sum_{m=-j}^{j}\mathcal{M}(m,u) = 1$. To compute the tomogram for a given direction with angles $\varphi = 0$ and θ, one has to estimate

$$\mathcal{M}(m,\theta) = \sum_{m'',m'=-j}^{j} u^*_{mm'}(\theta) f_m f^*_{m''} u_{m''m}(\theta), \tag{50}$$

where the matrix $u_{m''m}(\theta)$ is given by (46).

The following form for the matrix $u_{m'm}(\theta)$ is more convenient for numerical calculations:

$$u_{m'm}(\theta) = \left[\frac{(j+m')!(j-m')!}{(j+m)!(j-m)!}\right]^{1/2}\left(\cos\frac{\theta}{2}\right)^{m'+m}\left(\sin\frac{\theta}{2}\right)^{m'-m}P^{m'-m,m'+m}_{j-m'}(\cos\theta), \tag{51}$$

where $P^{a,b}_n$ are Jacobi polynomials.

In principle, one could use not only the unitary matrix in (46) but arbitrary unitary matrices. They contain a larger number of parameters (equal to N^2-1) and can provide additional information on the signal structure.

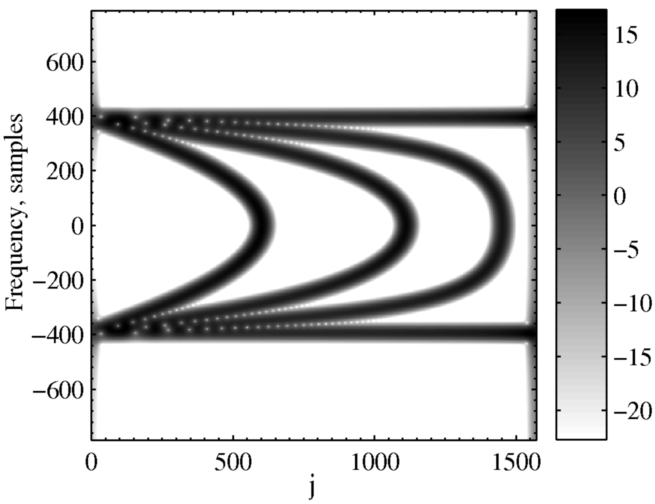

Fig. 5. Modulus of the short-time Fourier transform of the sum of four vectors of the rotated-time tomogram. Each $u_{m',0}(\theta, j)$ is a bent line in the time-frequency plane where θ fixes the size. Here $N = 1571$ and $\theta = \pi/8$, $2\pi/8$, $3\pi/8$, and $\pi/2$. As θ increases, the line is stretched to the right until it breaks in two parts for $\pi/2$.

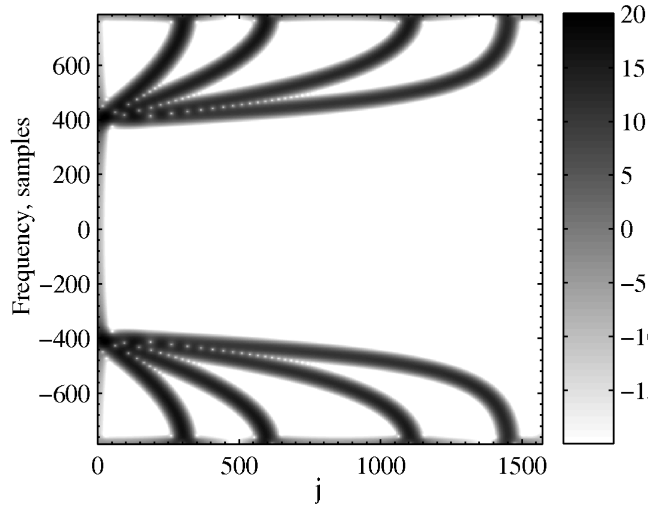

Fig. 6. Modulus of the short-time Fourier transform of the sum of four vectors of the rotated-time tomogram. Here $N = 1571$ and $\theta = 5\pi/8$, $6\pi/8$, $7\pi/8$, and $\pi - \pi/16$. Each $u_{m',0}(\theta, j)$ is made of two bent lines in the time–frequency plane, one in the upper-half plane and one in the lower-half plane.

How the time-rotated tomogram explores the time–frequency plane is, as before, illustrated by spectrograms of the eigenstates (Figs. 5 and 6). For $m = 0$, formula (51) reduces to the set of normalized associated Legendre functions $L_j^{m'}$,

$$u_{m',0}(\theta) = \sqrt{\frac{2}{2j+1}}L_j^{m'}(\cos\theta).$$

The normalized associated Legendre functions are related to the non-normalized ones $P_j^{m'}$ through

$$L_j^{m'}(\cos(\theta)) = \sqrt{\frac{2j+1}{2}\frac{(j-m')}{(j+m')}}P_j^{m'}(\cos\theta).$$

In the tomogram, θ is the parameter labeling the vectors of the basis associated to $m = 0$ and m'. The index j is the variable. In order to illustrate the effect of this tomogram, we computed numerically some vectors in the time–frequency plane (Figs. 5 and 6). In the discrete setting, if we choose $m' = N$, where N is the number of points, the $\{L_j^N\}_j$ form an orthonormal basis of the discrete time–frequency plane. Hence the projection on the eigenvectors of the rotated tomogram with $m = 0$ and $m' = N$ can be seen as the projection on bent lines in the time–frequency plane. This tomogram should be appropriate for studying the functions with similar symmetry properties in the time–frequency plane.

7. Hermite-Basis Tomography

Here we consider a dequantizer

$$\hat{U}(n,\alpha) = \hat{\mathcal{D}}(\alpha) \mid n\rangle\langle n \mid \hat{\mathcal{D}}^\dagger(\alpha), \qquad \alpha = |\alpha|e^{i\theta_\alpha} \tag{52}$$

and a quantizer

$$\hat{D}(n,\alpha) = \frac{4}{\pi(1-\lambda^2)} \left(\frac{\lambda+1}{\lambda-1}\right)^n \hat{\mathcal{D}}(\alpha) \left(\frac{\lambda-1}{\lambda+1}\right)^n \hat{\mathcal{D}}(-\alpha), \tag{53}$$

where $-1 < \lambda < 1$ is an arbitrary parameter and n is related to the order of an Hermite polynomial. This is analogous to the use of a photon-number basis in quantum optics.

For any signal $f(t)$, one has the probability distribution (tomogram)

$$\mathcal{M}_f(n,\alpha) = \mathrm{Tr}\ \mid f\rangle\langle f \mid \hat{U}(n,\alpha) \tag{54}$$

and, from the tomogram, the signal is reconstructed by

$$\mid f\rangle\langle f \mid = \sum_{n=0}^{\infty} \int d^2\alpha\, \mathcal{M}(n,\alpha)\hat{D}(n,\lambda). \tag{55}$$

One has $\mathcal{M}(n,\alpha) \geq 0$ and $\sum_{n=0}^{\infty} \mathcal{M}_f(n,\alpha) = 1$ for any complex α.

For an arbitrary operator $\hat{A}$, one has

$$\hat{I}\hat{A} = \sum_{n=0}^{\infty} \int d^2\alpha\, \hat{D}(n,\alpha)\mathrm{Tr}\left(\hat{U}(n,\alpha)\hat{A}\right), \tag{56}$$

where $\hat{I}$ is the identity operator.

The explicit form of the tomogram for a signal function $f(t)$ is

$$\mathcal{M}_f(n,\lambda) = \left|\langle f \mid \hat{\mathcal{D}}(\alpha) \mid n\rangle\right|^2 = \left|\int f^*(t) f_{n,\alpha}(t)\, dt\right|^2, \tag{57}$$

where

$$f_{n,\alpha}(t) = \hat{\mathcal{D}}(\alpha)\left[\pi^{-1/4}(2^n n!)^{-1/2} e^{-t^2/2} H_n(t)\right], \tag{58}$$

with $H_n(t)$ being an Hermite polynomial.

Thus, one has

$$f_{n,\alpha}(t) = \pi^{-1/4}(2^n n!)^{-1/2} e^{-(\alpha^2-\alpha^{*2})/4} e^{[(\alpha-\alpha^*)t]/\sqrt{2}} e^{-\tilde{t}^2/2} H_n(\tilde{t}) \tag{59}$$

and $\tilde{t} = t - (\alpha+\alpha^*)/\sqrt{2}$. For fixed $|\alpha|$, the tomogram is a function of the discrete set $n = 0, 1, \ldots$ and the phase factor θ_α.

How the Hermite-basis tomogram explores the time–frequency plane is, as before, illustrated by spectrograms of the eigenstates (Fig. 7). In the particular case where $\alpha = 0$, the functions $f_{n,0}$ are the Hermite functions. Their time–frequency representation has been calculated in Fig. 7. It shows that the tomogram at $\alpha = 0$ is suited for rotation-invariant functions in the time–frequency plane. One can see that for real α this pattern is shifted in time, and for purely imaginary α the pattern is shifted in frequency. The pattern can be shifted in both time and frequency by choosing the appropriate complex value for α.

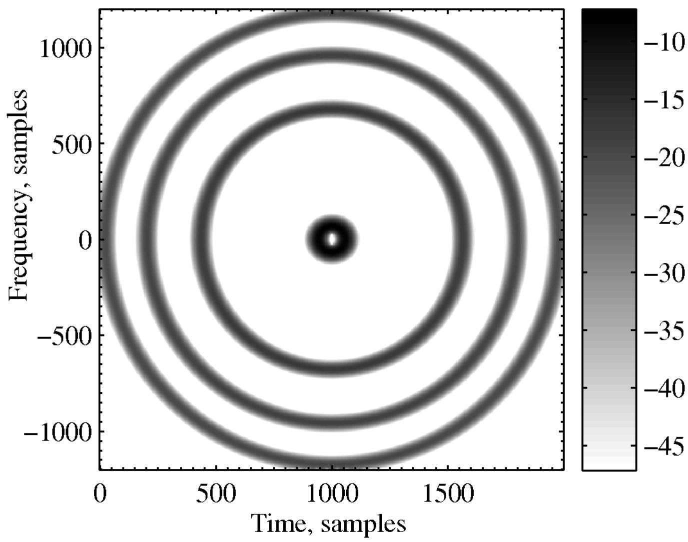

Fig. 7. Modulus of the short-time Fourier transform of the sum of four Hermite functions. Each ring is a Hermite function. Here, the number of points is $N = 2000$. The picture has been centered, the origin has been set to time $t = 1000$ and frequency $f = 0$. That is to say, $t = -N/2 + l\Delta t$ for $l \in [0, N)$ and $\Delta t = 1$. The smallest circle is for $n = 5$ and in increasing size order $n = 500$, $n = 1000$, and $n = 1500$, respectively.

8. Denoising, Component Separation, and Filtering

A few detailed applications of the tomograms associated to the operator $B(\mu,\nu) = \mu t + \nu\omega$ may already be found in the literature [14,20–23]. Here we simply include a few details of the methodology to be used by any type of tomogram to analyze complex signals. We also list the normalization modifications that are needed when dealing with finite-time signals. For example, for the time–frequency tomogram, instead of (24), we consider the finite-time tomogram, for a signal defined from t_0 to $t_0 + T$,

$$M_1(\theta, X) = \left| \int_{t_0}^{t_0+T} f^*(t)\psi^{(1)}_{\theta,X}(t)\, dt \right|^2 = \left| \langle f, \psi^{(1)} \rangle \right|^2, \tag{60}$$

with

$$\psi^{(1)}_{\theta,X}(t) = \frac{1}{\sqrt{T}} \exp\left(\frac{i\cos\theta}{2\sin\theta} t^2 - \frac{iX}{\sin\theta} t \right), \tag{61}$$

and $\mu = \cos\theta, \nu = \sin\theta$. Here, θ is a parameter that interpolates between the time and the frequency operators, running from 0 to $\pi/2$, whereas X is allowed to be any real number.

Likewise for the finite-time time–scale tomogram $M_2(\mu,\nu,X)$ [Eq. (25)] and the finite-time time–conformal tomogram $M_4(\mu,\nu,X)$ [Eq. (27)],

$$M_2(\theta, X) = \left| \int_{t_0}^{t_0+T} f^*(t)\psi^{(2)}_{\theta,X}(t)\, dt \right|^2 = \left| \langle f, \psi^{(2)} \rangle \right|^2, \tag{62}$$

$$\psi^{(2)}_{\theta,X}(t) = \frac{1}{\sqrt{\log|t_0+T| - \log|t_0|}} \frac{1}{\sqrt{|t|}} \exp i \left(\frac{\cos\theta}{\sin\theta} t - \frac{X}{\sin\theta} \log|t| \right), \tag{63}$$

$$X_n = X_0 + \frac{2n\pi}{\log|t_0+T| - \log|t_0|} \sin\theta, \qquad n \in \mathbb{Z}, \tag{64}$$

and

$$M_4(\theta, X) = \left| \int_{t_0}^{t_0+T} f^*(t)\psi^{(4)}_{\theta,X}(t)\, dt \right|^2 = \left| \langle f, \psi^{(4)} \rangle \right|^2, \tag{65}$$

$$\psi^{(4)}_{\theta,X}(t) = \sqrt{\frac{t_0(t_0+T)}{T}}\frac{1}{|t|}\exp i\left(\frac{\cos\theta}{\sin\theta}\ \log|t| + \frac{X}{t\sin\theta}\right), \tag{66}$$

$$X_n = X_0 + \frac{t_0(t_0+T)}{T}2\pi n\sin\theta, \qquad n\in\mathbb{Z}. \tag{67}$$

8.1. Denoising and Component Decomposition

Most natural and man-made signals are nonstationary and have a multicomponent structure. Therefore, separation of its components is an issue of great technological relevance. However, the concept of signal component is not uniquely defined. The notion of *component* depends as much on the observer as on the observed object. When we speak about a component of a signal we are, in fact, referring to a particular feature of the signal that we want to emphasize. For signals that have distinct features both in the time and the frequency domains, the time–frequency tomogram is an appropriate tool.

Consider finite-time tomograms as in (60). For all different θ's, the $U(\theta)$, of which $B(\theta)$ is the self-adjoint generator, are unitarily equivalent operators, hence all the tomograms share the same information.

First, we would select a subset X_n in such a way that the corresponding family $\left\{\psi^{(1)}_{\theta,X_n}(t)\right\}$ is orthogonal and normalized, $\langle\psi^{(1)}_{\theta,X_n}\psi^{(1)}_{\theta,X_m}\rangle = \delta_{m,n}$. This is possible by taking the sequence

$$X_n = X_0 + \frac{2n\pi}{T}\sin\theta, \qquad n\in\mathbb{Z}, \tag{68}$$

where X_0 is freely chosen (in general, we take $X_0 = 0$). We then consider the projections of the signal $f(t)$

$$c^{\theta}_{X_n}(f) = \langle f, \psi^{(1)}_{\theta,X_n}\rangle. \tag{69}$$

Denoising consists in eliminating the $c^{\theta}_{X_n}(f)$ such that $\left|c^{\theta}_{X_n}(f)\right|^2 \le \epsilon$ for some threshold ϵ. This power selective denoising is more robust than, for example, frequency filtering which may also eliminate important signal information.

The *component separation technique* is based on the search for an intermediate value of θ where a good compromise might be found between time localization and frequency information. This is achieved by selecting subsets $\mathcal{F}_k$ of the X_n and reconstructing partial signals (k-components) by restricting the sum to

$$f_k(t) = \sum_{n\in\mathcal{F}_k} c^{\theta}_{X_n}(f)\psi_{\theta,X_n}(t) \tag{70}$$

for each k. For examples and applications to experimental signals refer to [20–22].

If, in the linear combination $B(\mu,\nu) = \mu t + \nu O$, one chooses an operator O, that is specially tuned to the features of the signal that one wants to extract, then, by looking for the particular values of the set (μ,ν) where the noise effects cancel out, we may separate information of very small signals from large noise. This provides a signal-adapted filtering technique. The construction of the operator suited to particular signals may be done by the same techniques that are used in the bi-orthogonal decomposition [33].

9. Conclusions

Tomograms provide a two-variable characterization of signals which, due to its rigorous probabilistic interpretation, is robust and free of artifacts and ambiguities. For each particular signal that one wants to analyze, the choice of the appropriate tomogram depends not only on the signal but also on the features that we might want to identity or emphasize. So far we have explored component separation, denoising, and identification of small signal in noise, but other features may also benefit from the robust probabilistic nature of the tomographic analysis. This was our main motivation to include here a long list of many different operator choice leading to different classes of tomograms.

The description of the tomograms as operator symbols, with the corresponding quantizers and dequantizers, not only provides an alternative formulation but may also be used to extend the algebraic signal processing formalism to a wider nonlinear context.

Acknowledgments

V.I.M. thanks the Russian Foundation for Basic Research for partial support under Project No. 11-02-00456.

References

1. A. D. Poularikas (Ed.), *The Transforms and Applications Handbook*, CRC Press & IEEE Press, Boca Raton, Florida (1996).
2. K.-B. Wolf, *Integral Transforms in Science and Engineering*, Plenum Press, New York (1979).
3. J. B. J. Fourier, *Théorie Analytique de la Chaleur*, in: G. Darbous (Ed.), *Oeuvres de Fourier*, Gauthiers-Villars, Paris (1888), Tome premier.
4. J. M. Combes, A. Grossmann, and Ph. Tchamitchian (Eds.), *Wavelets*, 2nd ed., Springer, Berlin (1990).
5. I. Daubechies, "The wavelet transform: time–frequency localization and signal analysis," *IEEE Trans. Inform. Theory*, **36**, No. 5, 961–1005 (1990).
6. C. K. Chui (Ed.), *Wavelets: A Tutorial. Theory and Applications*, Academic, Boston (1992), Vol. 2.
7. E. Wigner, "On the quantum correction for thermodynamic equilibrium," *Phys. Rev.*, **40**, 749–759 (1932).
8. J. Ville, "Théorie et applications de la notion de signal analytique," *Cables et Transmission A*, **2**, 61–74 (1948).
9. L. Cohen, "Generalized phase-space distribution functions," *J. Math. Phys.*, **7**, 781–806 (1966).
10. L. Cohen, "Time–frequency distributions. A review," *Proc. IEEE*, **77**, 941–981 (1989).
11. S. Qian and D. Chen, *Joint Time–Frequency Analysis*, Prentice-Hall, Englewood Cliffs, New Jersy (1995).
12. K. Husimi, "Some formal properties of the density matrix," *Proc. Phys. Mat. Soc. Jpn*, **22**, 264–314 (1940).
13. Y. Kano, "A new phase-space distribution function in the statistical theory of the electromagnetic field," *J. Math. Phys.*, **6**, 1913–1915 (1965).
14. V. I. Man'ko and R. Vilela Mendes, "Noncommutative time–frequency tomography," *Phys. Lett. A*, **263**, 53–59 (1999).

15. M. A. Man'ko, V. I. Man'ko, and R. Vilela Mendes, "Tomograms and other transforms: A unified view," *J. Phys. A: Math. Gen.*, **34**, 8321–8332 (2001).
16. S. R. Deans, *The Radon Transform and Some of Its Applications*, John Wiley & Sons, New York (1983).
17. J. C. Woods and D. T. Barry, "Linear signal synthesis using the Radon–Wigner transform," *IEEE Trans. Signal Process.*, **42**, 2105–2111 (1994).
18. S. Granieri, W. D. Furlan, G. Saavedra, and P. Andrés, "Radon–Wigner display: a compact optical implementation with a single varifocal lens," *Appl. Opt.*, **36**, 8363–8369 (1997).
19. M. A. Man'ko, V. I. Man'ko, and R. V. Mendes, "A probabilistic operator symbol framework for quantum information," *J. Russ. Laser Res.*, Vol. 27, pp. 507–532 (2006).
20. F. Briolle, R. Lima, V. I. Man'ko, and R. Vilela Mendes, "A tomographic analysis of reflectometry data I: Component factorization," *Meas. Sci. Technol.*, **20**, 105501 (2009).
21. F. Briolle, R. Lima, and R. Vilela Mendes, "A tomographic analysis of reflectometry data II: The phase derivative," *Meas. Sci. Technol.*, **20**, 105502 (2009).
22. B. Ricaud, F. Briolle and F. Clairet, "Analysis and separation of time–frequency components in signals with chaotic behavior," `arXiv:1003.0734`.
23. C. Aguirre, P. Pascual, D. Campos, and E. Serrano, "Single neuron transient activity detection by means of tomography," *BMC Neuroscience 2011*, **12** (Suppl. 1), p. 297.
24. J. Bertrand and P. Bertrand, "A class of affine Wigner functions with extended covariance properties," *J. Math. Phys.*, **33**, 2515–2527 (1992).
25. P. Goncalvés and R. G. Baraniuk, "A pseudo-Bertrand distribution for time–scale analysis," *IEEE Signal Process. Lett.*, **3**, 82–84 (1996).
26. M. Asorey, P. Facchi, V. I. Man'ko, et al., "Generalized tomographic maps," *Phys. Rev. A*, **77**, 042115 (2008).
27. E. C. G. Sudarshan, "Equivalence of semiclassical and quantum-mechanical descriptions of statistical light beams," *Phys. Rev. Lett.*, **10**, 277–279 (1963).
28. R. J. Glauber, "Coherent and incoherent states of the radiation fields," *Phys. Rev.*, **131**, 2766–2788 (1963).
29. R. J. Glauber, "Photon correlations," *Phys. Rev. Lett.*, **10**, 84–86 (1963).
30. O. V. Man'ko, V. I. Man'ko, and G. Marmo, "Alternative commutation relation, star-products and tomography," *J. Phys. A: Math. Gen.*, **35**, 1–21 (2002).
31. M. Püschel and J. M. F. Moura, "Algebraic signal processing theory: Foundation and 1-D time," *IEEE Trans. Signal Process.*, **56**, 3572–3585 (2008).
32. M. Püschel and J. M. F. Moura, "Algebraic signal processing theory: 1-D space," *IEEE Trans. Signal Process.*, **56**, 3586–3599 (2008).
33. J. A. Dente, R. Vilela Mendes, A. Lambert, and R. Lima, "The bi-orthogonal decomposition in image processing: Signal analysis and texture segmentation," *Signal Process.: Image Commun.*, **8**, 131–148 (1996).